Physics Letters A 381 (2017) 3124–3128

Contents lists available at ScienceDirect

Physics Letters A

www.elsevier.com/locate/pla

Huge spin-transfer torque in a magnetic tunnel junction by a superlattice barrier

C.H. Chen, P. Tseng, C.W. Ko, W.J. Hsueh *

Nanomagnetism Group, Department of Engineering Science and Ocean Engineering, National Taiwan University, 1, Sec. 4, Roosevelt Road, Taipei, 10660, Taiwan

ARTICLE INFO

Article history:
Received 18 May 2017
Received in revised form 13 July 2017
Accepted 1 August 2017
Available online 7 August 2017
Communicated by M. Wu

Keywords:
Spintronics
Spin-polarized transport
Magnetic properties of heterostructures
Band structure

ABSTRACT

Huge spin-transfer torque (STT) in a magnetic tunnel junction (MTJ) achieved by superlattice barrier composed of alternate layers of a nonmagnetic metal and an insulator is proposed. The magnitude of the STT depends on the number of cells in the superlattice barrier and the nonmagnetic metal layer's thickness. The result shows that the STT of the novel superlattice-barrier MTJ can reach values up to four orders of magnitude greater than those of traditional single-barrier stacks based on three cells superlattice by designing the nonmagnetic metal layer's thickness. In addition, the spin-transfer torque of the proposed MTJ can also be thousands of magnitude greater than those of traditional double-barrier MTJs.

1. Introduction

Spintronics developed rapidly for systems such as metallic magnetic multilayers, magnetic semiconductors and strongly correlated electron systems [1,2]. Of these systems, magnetic tunnel junctions (MTJs), attracted widespread attention because of their potential applications in magnetic field sensors, nonvolatile magnetic random access memories (MRAMs) and other spintronic devices [3,4]. Current-induced magnetization switching (CIMS) is an important phenomenon in MTJ. The physics behind CIMS is the spin transfer from conduction electrons to localized magnetic moments, which results in an additional torque exerted on the film's magnetization. This torque is thus named the spin-transfer torque (STT), which has attracted much attention since its theoretical prediction [5,6] and experimental confirmation [7–10]. Potential STT applications include the STT-MRAMs, spin-torque nano-oscillators, spin-torque wave emitters, and spin-torque memristor [3,11]. The reduction of the critical current density is an important issue in the study of STT-MRAMs. For a typical single-barrier MTJ, the critical current density is usually in the order of 10^7 A/cm^2. For few-nanometer-thick barriers, a bias voltage of approximately 1 V is required to achieve this critical current density [12].

An artificial material, usually called superlattice, consists of two different materials, which can be chosen as copper and MgO, in regularly periodic arrangement with the nanoscopic scale thickness. Superlattices are used in different fields such as nanoelectronics [13–18], spintronics [19–22], and photonics [23–27]. Contrary to natural materials, superlattices can be more flexible for device design because their band structure can be tailored by adjusting their parameters. Recently, many studies have been proposed in experimental and theory of the STT superlattice-barrier MTJ [28–32]. Magnetic superlattices with special properties such as high magnetoresistance effect and magnonic bandgaps were proposed [19,22,33]. According to our previous study [19], the TMR ratio of the superlattice-barrier MTJ can be larger than that of the traditional single-barrier MTJ.

The STT effect in single-barrier (F/I/F) and double-barrier MTJs (F/I/F/I/F) was proposed [12,34–36], where F(I) denotes ferromagnet (insulator). In particular, the STT is approximately only one order of magnitude greater in the double-barrier MTJ when compared with the F/I/F single-barrier MTJ [12]. Recently, an F/I/N/I/F type double-barrier MTJ is proposed [37], where N denotes a nonmagnetic metal. The STT of this MTJ can be two orders of magnitude larger than that of traditional double-barrier MTJs. However, to the best of our knowledge, the STT effect has not yet been investigated in superlattice-barrier MTJs. Thus, taking advantage of the superlattice structure to enhance the STT in MTJs is of significant interest. It is well-known that the material of barrier has strong influence on the performance of MTJ. For instance, improvement of TMR ratio is achieved by replacing AlOx barrier by crystalline MgO. In this study, similarly, improvement of STT is achieved by replacing MgO with superlattice barrier. In this study, we show that by appropriately designing the forbidden and allowed bands in the superlattice barrier, the STT of the superlattice-barrier MTJ

* Corresponding author.
E-mail address: hsuehwj@ntu.edu.tw (W.J. Hsueh).

http://dx.doi.org/10.1016/j.physleta.2017.08.002
0375-9601/

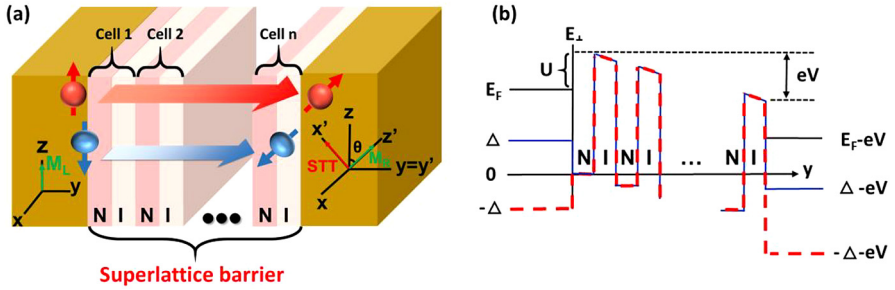

Fig. 1. (a) Schematic representation of an FP/(N/I)^n/F$_F$ superlattice-barrier MTJ. F$_{P(F)}$ stands for the pinned (free) layer, N(I) represents the nonmagnetic-metal (insulating) layer, and n denotes the number of cells in the superlattice barrier. M$_P$ and M$_F$ denote the magnetizations of the pinned and the free layer, respectively. (b) The potential profile of spin-up (red dashed line) and spin-down (blue solid line) electron for a superlattice-barrier MTJ with $n = 3$ in parallel configuration. (For interpretation of the references to color in this figure legend, the reader is referred to the web version of this article.)

can be four (three) orders larger than that of traditional single (double)-barrier stacks.

2. Model and formulation

Consider an MTJ with a superlattice-barrier structure comprising alternate binary nanometer-thick layers, a nonmagnetic metal layer, and an insulator layer with both sides enclosed by the pinned and free layers, as shown in Fig. 1(a). This superlattice-barrier MTJ is denoted as F$_P$/(N/I)^n/F$_F$, where F$_{P(F)}$ denotes the pinned (free) layer, N represents the nonmagnetic metal layer, and n denotes the number of cells in the superlattice barrier. The ferromagnet can be iron, cobalt or CoFeB etc. The non-magnetic metal layer can be copper. The insulator used in this study are assumed to be amorphous, such as amorphous AlOx or amorphous MgO. A bias voltage V is applied between the pinned and free layers. The two layers have a magnetization angle θ and are assumed to have sufficient thickness to be regarded as semi-infinite [38,39]. Two local coordinate systems are used in this study, and axial (x, y, z) for the pinned layer and layers in the superlattice barrier, including insulator layers and nonmagnetic metal layers, and axial (x', y', z') for the free layer. The z or z' axis follows the direction of the pinned or free layer magnetization, respectively. The y and y' axes are perpendicular to MTJ layers.

Slonczewski's parabolic band model [6,40] is adopted to calculate the electron transport in MTJs. Here, the inelastic scattering is considered in our model to analyze transport properties of electrons. When the thickness of nonmagnetic metal layer (d_N) in the superlattice-barrier MTJ is zero, the results for a traditional single-barrier MTJ of the form F/I/F can be obtained. The theoretical studies for the traditional single-barrier MTJ have been investigated in Ref. [39]. Our results for $d_N = 0$ nm are quite consistent with the results in this reference. Moreover, Wilczyński et al. have found that their results for in-plane torque in systems with semi-infinite electrodes roughly coincide with those presented in Ref. [38]. Most importantly, the theoretical predictions in this reference agree well with the experimental measurements [9]. The Schrödinger equation for the wave function for spin-up ($\psi_\uparrow$) and spin-down ($\psi_\downarrow$) electrons with an electron mass m can be written as

$$\left(-\frac{\hbar^2}{2m}\nabla^2 + U - \vec{\Delta}\cdot\vec{\sigma}\right)\begin{pmatrix}\psi_\uparrow\\ \psi_\downarrow\end{pmatrix} = E\begin{pmatrix}\psi_\uparrow\\ \psi_\downarrow\end{pmatrix}, \tag{1}$$

where U is the potential barrier height. $\vec{\Delta}$ is the molecular field caused by the exchange interaction [40]. The wave functions in layer j can be written as

$$\psi_j^\sigma(y) = A_j^\sigma e^{ik_j^\sigma(y-y_j)} + B_j^\sigma e^{-ik_j^\sigma(y-y_j)}, \tag{2}$$

where A_j^σ and B_j^σ are the amplitudes of the waves in the $+y$ and $-y$ directions, respectively. The superscript $\sigma = \pm 1$ or $(\sigma = \uparrow, \downarrow)$ denotes spin-up and spin-down electrons. When a bias is applied to an MTJ, the potential profile of insulator barriers becomes trapezoidal, as shown in Fig. 1(b). Insulator barriers inside the superlattice barrier are sliced into P rectangular barriers. The magnitude of the rectangular barriers is $U_p = (U + E_F) - p \cdot eV/P$, where $p = 1, 2, \ldots, P$ denotes the pth rectangular barrier counted from left to right. Note that the potential height U of the insulator is measured with reference to the Fermi energy. Wave vectors in the pinned and free layers are $k_{F_P}^\sigma = \sqrt{\frac{2m}{\hbar^2}(E_\perp + \sigma\Delta)}$ and $k_{F_F}^\sigma = \sqrt{\frac{2m}{\hbar^2}(E_\perp + \sigma\Delta - eV)}$, respectively, where $E_\perp$ is the transverse component of the total electron energy, given by $E_\perp = E - \hbar^2 k_{||}^2/2m$. Note that $E_\perp$ is measured with respect to the midpoint between the bottom portions of the two spin sub-bands in the pinned layer. The wave vectors are $k_I^\sigma = \sqrt{\frac{2m}{\hbar^2}(E_\perp - U_p)}$ in the insulator layer. In the wth nonmagnetic metal layer, the wave vectors are expressed as $k_N^\sigma = \sqrt{\frac{2m}{\hbar^2}(E_\perp - \frac{w-1}{n}\ \text{eV})}$. The wave function and its derivative must be continuous at all MTJ boundaries. Because of the quantization axis at the boundary between the rightmost insulator of the superlattice barrier and the free layer, the boundary condition is expressed as

$$\psi_I^\uparrow = \psi_{F_F}^\uparrow \cos(\theta/2) + \psi_{F_F}^\downarrow \sin(\theta/2) \quad \text{and} \tag{3a}$$

$$\psi_I^\downarrow = -\psi_{F_F}^\uparrow \sin(\theta/2) + \psi_{F_F}^\downarrow \cos(\theta/2). \tag{3b}$$

The amplitude of the electron wave function can then be calculated using the transfer-matrix method [41]. The μth component $(\mu = x, y, z)$ of the spin current density [42] can be expressed as $j_\mu^s(y) = \frac{i\hbar}{2m}\left[\left(\frac{\partial}{\partial y}\Psi^+(y)\right)\sigma_\mu\Psi(y) - \Psi^+(y)\sigma_\mu\left(\frac{\partial}{\partial y}\Psi(y)\right)\right]$, where $\Psi = \begin{bmatrix}\psi_\uparrow(y)\\ \psi_\downarrow(y)\end{bmatrix}$ is the wave function in spinor form and σ_μ is the Pauli matrix. The charge current density can be calculated from $j(y) = \frac{e\hbar}{m}\,\mathrm{Im}\sum_\sigma \psi_\sigma^*\left[\frac{d\psi_\sigma}{dy}\right]$. When a voltage bias V is applied to an MTJ, the total spin current density [39] in the zero temperature limit can be expressed as

$$J_\mu^s(y) = J_{\mu,1}^s(y) + J_{\mu,2}^s(y), \tag{4}$$

where $J_{\mu,1}^s(y)$ and $J_{\mu,2}^s(y)$ are the spin current densities contributed by electrons with an energy range of $[-\sigma\Delta, E_F - eV]$ and $[E_F - eV, E_F]$, respectively. $J_{\mu,1}^s(y)$ and $J_{\mu,2}^s(y)$ are expressed as

$$J_{\mu,1}^s(y) = \frac{4\pi^2 m^2}{h^4}\sum_\sigma \int_{-\sigma\Delta}^{E_F - \mathrm{eV}} dE_\perp \frac{eV}{k_{F_P}^\sigma(E_\perp)} j_\mu^s(y, E_\perp), \tag{5a}$$

$$J_{\mu,2}^s(y) = \frac{4\pi^2 m^2}{h^4}\sum_\sigma \int_{E_F - \mathrm{eV}}^{E_F} dE_\perp \frac{E_F - E_\perp}{k_{F_P}^\sigma(E_\perp)} j_\mu^s(y, E_\perp). \tag{5b}$$

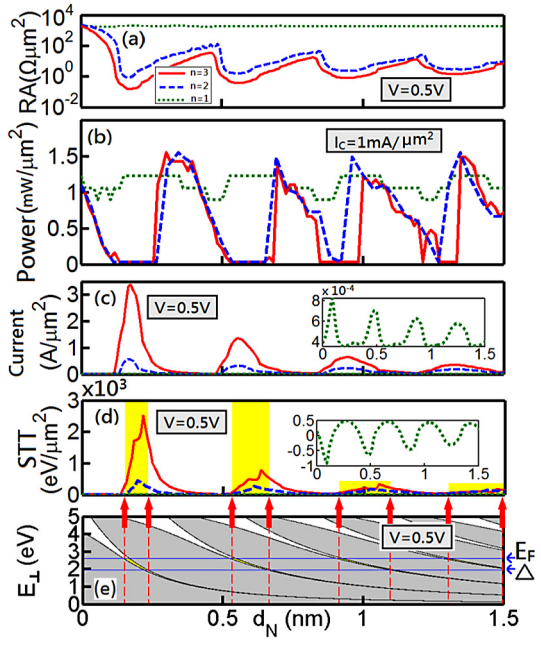

Fig. 2. The effect of nonmagnetic metal layer thickness on (a) RA, (b) power, (c) charge current density and (d) STT of the $F_P/(N/I)^n/F_F$ superlattice-barrier MTJ, and (e) band structure of the superlattice barrier. The yellow region denotes the range of d_N that provides an allowed band within the energy range (Δ, E_F). The parameters used for the simulation are the spin-splitting energy $\Delta = 1.96$ eV, Fermi energy, $E_F = 2.62$ eV, height of the insulator layer, $U = 1.5$ eV, bias voltage, $V = 0.5$ V, angle between the magnetization of pinned layer and free layer, $\theta = \pi/2$ and the insulator layer thickness, $d_I = (1/n)$ nm. (For interpretation of the references to color in this figure legend, the reader is referred to the web version of this article.)

The STT exerted per unit square of the free layer [39] can be expressed as $\mathrm{STT} = -\frac{\hbar}{2} J^s_{x'}$, where $J^s_{x'}$ is the x'-component of the spin current density. The charge current density can be obtained by replacing j^s_μ with $j(y)$. The band structure of the superlattice barrier is calculated using the periodic boundary [37]. The wave functions in the system with a periodic boundary must obey the Bloch waves. Therefore, the dispersion relation $\cos(KL)$ of the superlattice barrier can be obtained, where K is the Bloch wave number and L is the width of a unit cell.

First, we study the effect of the change in the superlattice barrier number of cell (n) and the thickness of the nonmagnetic layer (d_N) on the resistance-area product (RA), the power consumption, the charge current density and STT of the superlattice-barrier MTJ. The relevant parameters for iron are the Fermi energy $E_F = 2.62$ eV and the spin-splitting energy $\Delta = 1.96$ eV, which is widely used in MTJ modeling [39]. For an insulating barrier, the potential height and insulator thickness are $U = 1.5$ eV and $d_I = (1/n)$ nm, respectively. The RA and power consumption as a function of d_N is plotted, as shown in Figs. 2(a–b). The critical current for magnetization switching is assumed to be fixed at $I_C = 1$ mA/μm^2. The power for superlattice-barrier MTJ can be lower than that of the traditional single-barrier MTJ at certain d_N. The improvement can be attributed to the resonant tunneling [19,43] formed in the superlattice barrier. For a single-barrier structure, there is no resonant tunneling such that the RA is large. Larger power is required to achieve critical current. In contrast, the resonant tunneling formed in the superlattice-barrier such that the RA is lower. Therefore, lower power is required to achieve critical current in the superlattice-barrier MTJ.

The charge current density and the STT of the superlattice-barrier MTJ as a function of d_N for different superlattice-barrier numbers of cells appear in Figs. 2 (c) and (d). A bias voltage $V = 0.5$ V is applied to the structure. In this case, electrons tunnel

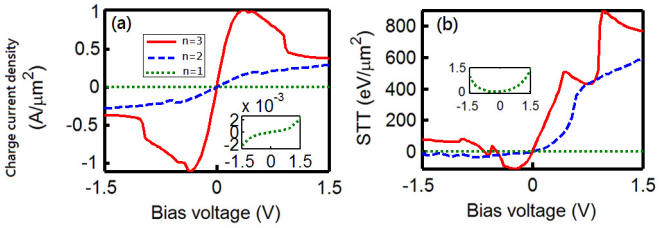

Fig. 3. Bias dependence of the (a) charge current density and (b) STT for three different numbers of cells in the superlattice barrier. The inset in each figure shows an enlarged view of the plot for $n = 1$. The other parameters of the junction are the same as those in Fig. 2, except that $d_N = 0.6$ nm.

from the pinned to free layer. As shown in Figs. 2(c–d), the charge current density and STT are strongly influenced by the thickness of the nonmagnetic metal layer for the three different number of cells. In fact, they oscillate as d_N increases. Several peaks are observed in Figs. 2(c–d). For thicker d_N, the magnitude of these peaks decreases, whereas their width increases. For $n = 1$, the MTJ is similar to the traditional single-barrier MTJ [39]. With increasing n, the magnitude of these peaks increases. For $n = 2$, the MTJ structure becomes F/N/I/N/I/F, which is similar to a double-barrier structure. The STT of this MTJ can be three orders of magnitude larger than traditional single-barrier MTJs at certain d_N. Some studies [12] showed that the STT of an F/I/F/I/F double-barrier MTJ is only approximately one order of magnitude larger than that of a single-barrier MTJ. In other words, the STT of the F/N/I/N/I/F MTJ can be two orders of magnitude larger than that of traditional F/I/F/I/F double-barrier MTJ. For $n = 3$, the STT is four (one) orders of magnitude larger than that of the MTJ with $n = 1$ $(n = 2)$. This phenomenon can be attributed to the formed band structure of the superlattice barrier, as discussed below.

Since the STT is highly dependent on the superlattice-barrier structure, it is interesting to see how the band structure of the superlattice-barrier is related to the STT. Fig. 2(e) shows the band structure of the superlattice barrier. The allowed band within the energy range $[\Delta, E_F]$ is colored yellow. The corresponding d_N for this energy range is the thickness where peaks of the STT can be found (Fig. 2d). Therefore, the band structure of the superlattice barrier with two parameters obtained from the ferromagnetic electrodes, Δ and E_F, can be used to predict the thicknesses required for a large charge current density and STT to occur.

In addition, we investigate the bias dependence of the charge current density and the STT, as shown in Fig. 3. The parameters are the same as those used in Fig. 2, except for the thickness of the nonmagnetic metal, which is set at $d_N = 0.6$ nm, so that a large charge current density and STT occurs. For $n = 1$, the MTJ is similar to the traditional single-barrier MTJ. The charge current density gradually increases as the applied voltage increases, as shown in the inset of Fig. 3(a), similar to the single-barrier MTJ [39]. However, with increasing n, the charge current density no longer increases monotonically with the applied voltage. An significant negative differential resistance is observed at $V = 0.5$ V. Similar effect has been observed in the magnetic multilayer systems [44]. Fig. 3(b) shows the STT as a function of the applied voltage for different numbers of cells. For $n = 1$, the STT decreases monotonically as applied voltage changes from -1.5 V to 0 V and increases monotonically as applied voltage changes from 0 V to 1.5 V. The STT is asymmetric with respect to the bias reversal, even in junctions with both identical electrodes, in agreement with both experiment and calculation results for single-barrier MTJ [9,39,45]. This asymmetric property holds for $n > 1$. However, the characteristics of the STT become more complex. In the small bias range (in this case, $|V| < 0.3$ V), the STT characteristics STT for MTJs with $n = 3$ are similar to those for the single-barrier MTJs. However, for a larger bias voltage, the curve no longer changes monotonically.

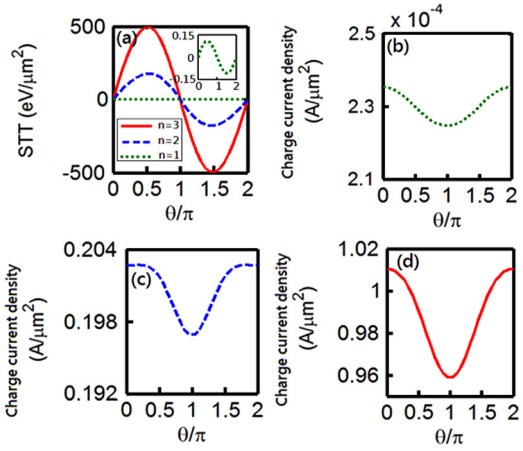

Fig. 4. (a) The STT as a function of θ for $n = 1, 2$ and 3. Plot of charge current density as a function of θ for superlattice-barrier MTJs. The parameters are the same as those used in Fig. 2. The inset in (a) shows an enlarged view of the case for $n = 1$. The applied voltage is $V = 0.5$ V.

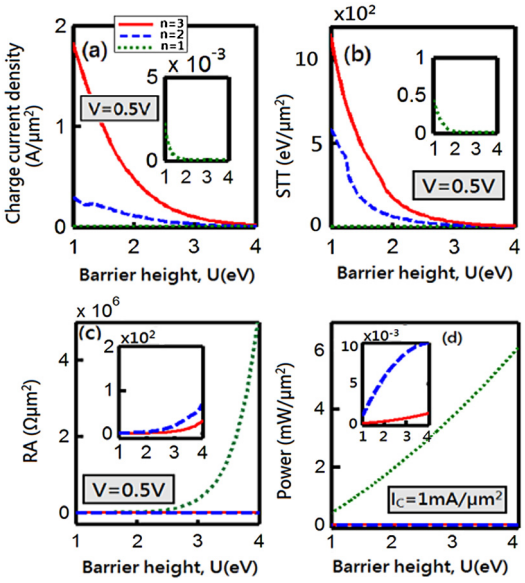

Fig. 5. Trend in the (a) charge current density, (b) STT, (c) RA and (d) power as a function of the barrier height. The parameters are the same as those used in Fig. 2. The inset is a partially enlarged view of the trend corresponding to $d_N = 0$ nm.

Furthermore, we study the effect of the angle θ between the magnetic moments of the electrodes on the charge current density and the STT, as shown in Fig. 4. For $n = 1$, the STT reaches a maximum absolute value for $\theta = \pi/2$ and $\theta = 3\pi/2$, and is zero in the collinear configuration. This phenomenon is similar to that of the single-barrier MTJ. This can be expected, since the STT of the superlattice-barrier MTJ with $n = 1$ is quite similar to that of the traditional single-barrier MTJ. In the superlattice-barrier MTJ, the features of the STT are quite similar to those in the single-barrier MTJ, except for the magnitude of the torque. The maximum STT increases with the number of cells in the superlattice barrier, consistently with the discussion for Fig. 2. Figs. 4 (b)–(d) show the charge current densities for the three different number of cells. For $n = 1$, the charge current density is maximal in the parallel configuration and monotonically decreases when magnetic moments rotate towards the anti-parallel configuration. The same trend is observed for increasing n. The charge current density for the MTJ with $n = 2$ is about three orders of magnitude larger than that for the MTJ with $n = 1$. The charge current density of the MTJ with $n = 3$ is about one order of magnitude larger than that of the MTJ with $n = 2$. Therefore, the charge current density and the STT can be increased by increasing the number of cells in the superlattice barrier.

The effect of the barrier height on the charge current density, STT, RA and power is studied, as shown in Fig. 5. For different number of cells, the charge current density decreases with increasing barrier height, as shown in Fig. 5(a). However, the charge current is greater for MTJs with larger numbers of cells, especially when the barrier height is small. A similar phenomenon is observed for the effect of barrier height on the STT, as shown in Fig. 5(b). The RA and power increases for increasing barrier height, as shown Fig. 5(c) and Fig. 5(d). The power and RA for $n = 2$ and $n = 3$ superlattice-barrier MTJ are greatly improved as compared with the single-barrier MTJ.

In conclusion, the charge current density and the STT can be enhanced using superlattice barrier. Indeed, the magnitudes of the charge current density and the STT are proportional to the number of cells in the superlattice barrier. The STT and the charge current density of this novel superlattice-barrier MTJ with $n = 3$ can be about four (three) orders of magnitude larger than those of the traditional single- (double-) barrier MTJ, if the thickness of the nonmagnetic metal layer in the superlattice-barrier is properly designed. This improvement can be attributed to allowed and forbidden bands formed in the superlattice barrier.

Acknowledgement

The authors acknowledge the support provided by the Ministry of Science and Technology of Taiwan, under grant numbers MOST 104-3113-E-002-001 and MOST 105-2221-E-002-136.

References

[1] I. Žutić, J. Fabian, S. Das Sarma, Rev. Mod. Phys. 76 (2004) 323–410.
[2] P. Němec, V. Novák, N. Tesařová, E. Rozkotová, H. Reichlová, D. Butkovičová, F. Trojánek, K. Olejník, P. Malý, R.P. Campion, B.L. Gallagher, J. Sinova, T. Jungwirth, Nat. Commun. 4 (2013) 1422.
[3] N. Locatelli, V. Cros, J. Grollier, Nat. Mater. 13 (2014) 11–20.
[4] C. Chappert, A. Fert, F.N.V. Dau, Nat. Mater. 6 (2007) 813–823.
[5] L. Berger, Phys. Rev. B 54 (1996) 9353–9358.
[6] J.C. Slonczewski, J. Magn. Magn. Mater. 159 (1996) L1–L7.
[7] C. Wang, Y.T. Cui, J.Z. Sun, J.A. Katine, R.A. Buhrman, D.C. Ralph, Phys. Rev. B 79 (2009) 224416.
[8] J.A. Katine, F.J. Albert, R.A. Buhrman, E.B. Myers, D.C. Ralph, Phys. Rev. Lett. 84 (2000) 3149–3152.
[9] H. Kubota, A. Fukushima, K. Yakushiji, T. Nagahama, S. Yuasa, K. Ando, H. Maehara, Y. Nagamine, K. Tsunekawa, D.D. Djayaprawira, N. Watanabe, Y. Suzuki, Nat. Phys. 4 (2008) 37–41.
[10] S.I. Kiselev, J.C. Sankey, I.N. Krivorotov, N.C. Emley, R.J. Schoelkopf, R.A. Buhrman, D.C. Ralph, Nature 425 (2003) 380–383.
[11] V. Sluka, A. Kákay, A.M. Deac, D.E. Bürgler, C.M. Schneider, R. Hertel, Nat. Commun. 6 (2015) 6409.
[12] N.N. Mojumder, C. Augustine, D.E. Nikonov, K. Roy, J. Appl. Phys. 108 (2010) 104306.
[13] C.H. Chang, C.W. Tsao, W.J. Hsueh, New J. Phys. 16 (2014) 113069.
[14] A.K. Yadav, C.T. Nelson, S.L. Hsu, Z. Hong, J.D. Clarkson, C.M. Schlepütz, A.R. Damodaran, P. Shafer, E. Arenholz, L.R. Dedon, D. Chen, A. Vishwanath, A.M. Minor, L.Q. Chen, J.F. Scott, L.W. Martin, R. Ramesh, Nature 530 (2016) 198–201.
[15] M.P. Boneschanscher, W.H. Evers, J.J. Geuchies, T. Altantzis, B. Goris, F.T. Rabouw, S.A.P. van Rossum, H.S.J. van der Zant, L.D.A. Siebbeles, G. Van Tendeloo, I. Swart, J. Hilhorst, A.V. Petukhov, S. Bals, D. Vanmaekelbergh, Science 344 (2014) 1377–1380.
[16] D.Z.-Y. Ting, A. Soibel, A. Khoshakhlagh, J. Nguyen, L. Höglund, S.A. Keo, J.M. Mumolo, S.D. Gunapala, Appl. Phys. Lett. 102 (2013) 121109.
[17] G. Ye, H. Wang, S. Arulkumaran, G.I. Ng, R. Hofstetter, Y. Li, M.J. Anand, K.S. Ang, Y.K.T. Maung, S.C. Foo, Appl. Phys. Lett. 103 (2013) 142109.
[18] W. Yang, G. Chen, Z. Shi, C.-C. Liu, L. Zhang, G. Xie, M. Cheng, D. Wang, R. Yang, D. Shi, K. Watanabe, T. Taniguchi, Y. Yao, Y. Zhang, G. Zhang, Nat. Mater. 12 (2013) 792–797.
[19] C.H. Chen, W.J. Hsueh, Appl. Phys. Lett. 104 (2014) 042405.
[20] M.N. Baibich, J.M. Broto, A. Fert, F.N. Van Dau, F. Petroff, P. Etienne, G. Creuzet, A. Friederich, J. Chazelas, Phys. Rev. Lett. 61 (1988) 2472–2475.
[21] S.V. Grishin, E.N. Beginin, Y.P. Sharaevskii, S.A. Nikitov, Appl. Phys. Lett. 103 (2013) 053908.

[22] B. Lenk, H. Ulrichs, F. Garbs, M. Münzenberg, Phys. Rep. 507 (2011) 107–136.
[23] Y.H. Cheng, C.H. Chang, C.H. Chen, W.J. Hsueh, Phys. Rev. A 90 (2014) 023830.
[24] Y. Fink, J.N. Winn, S. Fan, C. Chen, J. Michel, J.D. Joannopoulos, E.L. Thomas, Science 282 (1998) 1679–1682.
[25] Q. Xie, C. Lee, Phys. Rev. A 85 (2012) 063802.
[26] W.J. Hsueh, C.T. Chen, C.H. Chen, Phys. Rev. A 78 (2008) 013836.
[27] C.S.R. Kaipa, A.B. Yakovlev, G.W. Hanson, Y.R. Padooru, F. Medina, F. Mesa, Phys. Rev. B 85 (2012) 245407.
[28] Q.L. Ma, X.M. Zhang, T. Miyazaki, S. Mizukami, Sci. Rep. 5 (2015) 7863.
[29] Y. Kay, F. Akio, K. Hitoshi, K. Makoto, Y. Shinji, Appl. Phys. Express 6 (2013) 113006.
[30] A.O. León, M.G. Clerc, S. Coulibaly, Phys. Rev. E 89 (2014) 022908.
[31] J.-H. Han, H.-W. Lee, Phys. Rev. B 86 (2012) 174426.
[32] T. Qu, S.C. Pandey, G.S. Sandhu, R.H. Victora, IEEE Trans. Magn. 52 (2016) 1–5.
[33] T. Valet, A. Fert, Phys. Rev. B 48 (1993) 7099–7113.
[34] Z. Diao, A. Panchula, Y. Ding, M. Pakala, S. Wang, Z. Li, D. Apalkov, H. Nagai, A. Driskill-Smith, L.-C. Wang, E. Chen, Y. Huai, Appl. Phys. Lett. 90 (2007) 132508.
[35] I. Theodonis, A. Kalitsov, N. Kioussis, J. Magn. Magn. Mater. 310 (2007) 2043–2045.
[36] A. Vedyayev, N. Ryzhanova, B. Dieny, N. Strelkov, Phys. Lett. A 355 (2006) 243–246.
[37] C.H. Chen, Y.H. Cheng, J.W. Ko, W.J. Hsueh, Appl. Phys. Lett. 107 (2015) 152401.
[38] I. Theodonis, N. Kioussis, A. Kalitsov, M. Chshiev, W.H. Butler, Phys. Rev. Lett. 97 (2006) 237205.
[39] M. Wilczyński, J. Barnaś, R. Świrkowicz, Phys. Rev. B 77 (2008) 054434.
[40] J.C. Slonczewski, Phys. Rev. B 39 (1989) 6995–7002.
[41] M. Steęślicka, R. Kucharczyk, A. Akjouj, B. Djafari-Rouhani, L. Dobrzynski, S.G. Davison, Surf. Sci. Rep. 47 (2002) 93–196.
[42] M. Wilczyński, J. Magn. Magn. Mater. 325 (2013) 94–101.
[43] C.H. Chen, Y.H. Cheng, W.J. Hsueh, Europhys. Lett. 111 (2015) 47005.
[44] J. Munárriz, C. Gaul, A.V. Malyshev, P.A. Orellana, C.A. Müller, F. Domínguez-Adame, Phys. Rev. B 88 (2013) 155423.
[45] I. Theodonis, A. Kalitsov, N. Kioussis, Phys. Rev. B 76 (2007) 224406.